Near-real-time feature-selective modulations in human cortex

Javier O. Garcia[1,*], **Ramesh Srinivasan**[2], and **John T. Serences**[1,3,*]

[1]Department of Psychology, 9500 Gilman Dr., University of California San Diego, La Jolla, CA 92093-0109

[2]Department of Cognitive Sciences, University of California Irvine, Irvine, California 92697-5100

[3]Neuroscience Graduate Program, University of California San Diego, La Jolla, CA 92093-0109

SUMMARY

In order to link neural activity with cognitive function, information is needed about both the temporal dynamics and the content of neural codes. Traditionally, recording single neurons in animals has been the primary means of obtaining high temporal resolution as well as precise information about neural tuning properties such as selectivity for different sensory features. Recent fMRI studies in humans have been able to measure feature selectivity within specific sub-regions of sensory cortex (e.g., orientation selectivity in primary visual cortex, or V1) [1, 2]. However, investigating the neural mechanisms that support cognitive processing – which often occur rapidly on a sub-second scale – using a temporally insensitive method such as fMRI severely limits the types of inferences that can be drawn. Here, we describe a new method for tracking the rapid temporal evolution of feature-selective information processing with scalp recordings of EEG. We generate orientation-selective response profiles based on the spatially distributed pattern of steady-state visual evoked potential (SSVEP) responses to flickering visual stimuli. Using this approach, we report a multiplicative attentional modulation of these feature-selective response profiles with a temporal resolution of 24ms–120 ms, which is far faster than that achieved using fMRI. Finally, we show that behavioral performance on a discrimination task can be predicted based on the amplitude of these temporally precise feature-selective response profiles. This method thus provides a high temporal resolution metric that can be used to track the influence of cognitive manipulations on feature-selective information processing in human cortex.

Keywords

EEG; attention; decoding model; encoding model; vision

RESULTS AND DISCUSSION

Sensory systems operate via the joint activity of millions of neurons that are tuned to different stimulus attributes, and the tuning of these neurons becomes increasingly complex as information is relayed through successive stages of processing [3, 4]. For example, many neurons in the retina respond most strongly to small spots of light, many neurons in early areas of visual cortex (e.g., primary visual cortex) respond most strongly to oriented lines, and neurons at later stages of visual cortex respond most strongly to complex objects such as

*Corresponding Author: Javier O. Garcia or John T. Serences, javiergarcia@ucsd.edu, jserences@ucsd.edu.

faces [5, 6]. As a result of this neural selectivity, and the fact that decisions based on sensory inputs can often be made in hundreds of milliseconds, understanding the computational principles that underlie neural information processing requires both sensitivity to the stimulus attributes being processed (feature selectivity) and high temporal resolution. Over the last several decades, electroencephalography (EEG) and magnetoencephalography (MEG) have primarily been used to achieve a high temporal resolution [e.g, 7, 8, 9], whereas fMRI has primarily been used to achieve a high degree of feature selectivity [e.g., 10, 11, 12]. However, few studies have attempted to make inferences at both levels of analysis, thus placing severe constraints on our understanding of information processing in human cortex.

Recently, many studies have exploited changes in multivariate patterns of activation across fMRI images to recover feature-selective responses in human visual cortex (multivariate pattern analysis, or MVPA, methods) [1, 11–14]. For instance, fluctuations in activation patterns within early visual areas can be used to predict the specific orientation of a stimulus being viewed by a subject [1, 15]. The systematic orientation-dependent modulation of voxel responses within these early visual areas is thought to be driven by small modulations in neural activity at the columnar level (~300–500μm) [1, 16] and by modulations across larger-scale maps of orientation that are arrayed across early areas of the visual system such as V1 [17].

These relatively new multivariate approaches to fMRI image analysis fall into two broad categories. *Decoding* analyses use machine learning algorithms to estimate which specific stimulus – selected from a larger set of possible stimuli – was most likely to have been viewed based on an observed pattern of activation. To the extent that these algorithms can correctly guess the stimulus label, one can infer that some stimulus-specific information is being encoded in the cortical region of interest [11–13, 18]. However, while decoding analyses are very sensitive to changes in the information content of a cortical area, they do not directly reveal *how* changes in patterns of neural activity give rise to separable activation patterns at the macroscopic level afforded by fMRI. Thus, to complement decoding models, recent studies have employed *encoding* models that use a priori assumptions about different feature spaces – such as the well known orientation selectivity of neurons in primary visual cortex [19, 20] – to make inferences about how experimental manipulations change population-level neural response profiles. These forward encoding models have been used to reconstruct novel visual stimuli [21], to investigate color- and orientation-selective responses in early visual cortex [2, 22, 23], and to examine the effects of feature-based attention on the shape of orientation selective response profiles in primary visual cortex [24].

Despite these advances, BOLD neuroimaging has inherently poor temporal resolution on the order of several seconds, and can subsequently reveal little about the dynamics of neural information processing. Here, we combine decoding and encoding models with EEG to determine if more precise temporal information can be recovered about feature-selective modulations in human cortex, and to determine if any observed feature-selective modulations are sensitive to task demands. To this end, we designed a behavioral task to examine orientation-selective responses under conditions of focused or withdrawn attention. Subjects viewed a visual display containing a square-wave orientated grating rendered in a large circular annulus and a rapid serial visual presentation (RSVP) stream of letters that was presented within the annulus at fixation (Figures 1A,B). On half of the trials, subjects attended the peripheral grating and pressed a button when they detected a clockwise (CW) or a counter clockwise (CCW) shift in the orientation of the grating. On the other half of the trials, subjects ignored the peripheral grating and pressed a button whenever they detected a pre-specified target letter in the central RSVP stream. To delineate neural responses

separately for each stimulus (grating versus RSVP stream), stimuli were *tagged* with different flicker frequencies: the contrast of the peripheral grating was reversed at 21.25 Hz, and the RSVP stream of letters was updated at a rate of 12.1 Hz. Steady state visual evoked potentials (SSVEPs) were estimated using a Fourier analysis to separately assess the response to each stimulus. We focused our analyses on the magnitude of the second harmonic of the flickering grating (42.5 Hz) and the magnitude of first harmonic of the flickering RSVP stream, consistent with known differences in contrast-reversed and luminance-defined SSVEPs (see Figure 3A for full spectra and stimulus related activity across time) [25]. The dominant response at twice the reversal frequency (42.5 Hz) of the orientation grating elicited a focal response with a peak over the parietal-occipital region. Peak average responses span from electrodes corresponding to POz to Pz (posterior to anterior) and P1 to PO4 (left to right), with largest amplitude centered at Pz (In descending SNR: Pz, PO4, POz, P2, P1). The 12.1 Hz response to the RSVP stream, however, had a bilateral spatial distribution with peaks in parietal cortex (Figure 1C).

We first used a linear classifier to determine if stimulus orientation could be decoded based on the spatial distribution of the signal-to-noise ratio (SNR) and the phase of the SSVEP response at 42.5Hz across selected electrodes [see Supplemental Experimental Procedures, *SSVEP Responses*]. Classification accuracy for orientation was significantly above chance even when subjects were attending to the central RSVP stream (blue bars in Figure 2A; $p < 0.05$, note that this and all other p-values computed via a bootstrapping procedure, see Supplemental Experimental Procedures and Supplemental Figure 4). Moreover, classification accuracy increased significantly when subjects attended to the oriented grating, demonstrating that the orientation selective patterns of SSVEP were sensitive to task demands ($p < 0.05$, Figure 2A). In contrast, the power and phase of the SSVEP responses evoked by the RSVP stream (12.1 Hz) could not be used to decode the orientation of the stimulus (red bars in Figure 2A; $p > 0.05$). The EEG electrodes that contained the highest SNR were also the most diagnostic for this analysis (Figure 2B).

Having established that the spatial distribution of SSVEP power and phase can be used to successfully *decode* the angle of the orientated grating, we next considered whether the power and phase could also be used to reconstruct a population-level representation of the orientation-selective neural activity (i.e. a population-level orientation tuning function, or TF). We used a linear forward encoding model that has been previously used to estimate feature-selective tuning functions using fMRI [2, 22, 26, 27]. In short, we estimated the magnitude of the response in each electrode as a linearly weighted sum of the idealized orientation tuning functions shown in Figure 2C. Using these weights, we then estimated the relative magnitude of the SSVEP response within different sub-populations of neurons (or 'channels') that are tuned to different orientations (see Experimental Procedures).

We first established the effectiveness of this technique when applied to the power and phase of the SSVEP response at 42.5 Hz based on a Fourier analysis of the data from the entire interval before the onset of the target. Only data collected prior to target onset were used to avoid contamination by responses to the rotation of the grating either clockwise or counter-clockwise (CW/CCW). The enhanced response to neural populations tuned to the orientation of the stimulus being viewed, accompanied by the characteristic Gaussian drop off in the signal associated with neural populations tuned successively farther away, demonstrates that SSVEP power and phase can be used to estimate the shape of feature-selective population response profiles in human cortex (Figure 2D). Moreover, projecting the data from electrode space into orientation channel space does not significantly degrade the amount of orientation-selective information, as linear classification performed on single trial tuning functions is well above chance (21.8% collapsed across all conditions).

We next examined the extent to which each electrode contributed to these feature-selective population TFs. Perhaps not surprisingly based on the SNR plots in Figure 1C, power fluctuations in a relatively focal set of occipital-parietal electrodes carried most of the orientation-selective information (Figure 2E). The orientation-selective modulation of phase, on the other hand, was most evident in electrodes over frontal cortex; however, phase contributed far less information to the orientation-selective TFs shown in Figure 2E(see also Supplemental Figure 1A).

As a control analysis, we also attempted to generate orientation-selective TFs based on the power and phase of the SSVEPs associated with the RSVP stream (12.1 Hz). We were not able to compute feature-selective TFs based on the response associated with the RSVP stream, irrespective of whether the subject was attending the RSVP stream or the peripheral grating. Thus, the feature-selective population response profiles shown in Figure 2 are specific to the neural response associated with the flickering grating. Finally, we also inspected individual electrode tuning functions (Supplemental Figure 1B) and noted fluctuations in each electrode as a function of stimulus orientation with no substantial changes in overall mean response amplitude. This implies that feature selectivity is driven by aggregating weak orientation selective signals across electrodes.

As the data presented thus far relied on the power and phase of the SSVEPs across a large time window (the entire pre-target window), we next evaluated the temporal precision with which we could measure orientation-selective response profiles. We used a wavelet that was progressively shifted across time in 1ms intervals to compute the power and phase of the SSVEP response at 42.5 Hz (Figure 3A). Note that even though we sampled at 1000 Hz, the smallest meaningful unit of time in this study is one stimulus cycle, or 24 ms, which provides the upper limit on our temporal resolution. Moreover, the Gaussian window of the wavelet effectively averages over a slightly larger temporal window spanning five cycles of the flickering grating (or 120 ms). Thus, the temporal resolution is between 24 ms and 120 ms, and will vary as a function of the temporal bandwidth of the Gaussian envelope and the flicker frequency of the stimulus.

This analysis revealed dynamic TFs (DTFs) that were sensitive to both behavioral performance and task demands (Figure 3). For example, these DTFs reveal a sustained multiplicative increase in amplitude when subjects were attending to the peripheral grating compared to when they were attending to the central RSVP stream (Figure 3B, 3C). Moreover, during trials in which the peripheral grating was attended, the DTFs were significantly higher in the pre-target interval on correct compared to incorrect trials (Figure 3D, 3E, 4C). This increase in the gain of the DTFs on correct trials is apparent across the entire 500ms interval before target onset. We confirmed these effects were not driven by the fact that an error was made on only ~20% of all trials by observing the same effect when we randomly sampled subsets of the correct trials (Supplemental Figure 2).

A closer inspection of the DTFs derived from correct trials also reveals rapid changes in the magnitude of the response profiles immediately before and after the target onset (Figure 4). To characterize the differences between the conditions, we inspected DTFs across a 200 ms window before the onset of the target (Figure 4B). When subjects were attending to the oriented grating, the pre-target interval shows a significantly larger response at −20°, 0°, and 20° channel offsets on attended compared to unattended trials. In Figure 4C, we compare correct and incorrect trials (of only attend-grating trials). The difference between correct and incorrect trials is most reliable at −20° and 20° channel offsets (also visible at 0°) within the pre-target interval. Furthermore, the orientation shift of the grating (the appearance of the target) is visible in the channel responses across time. Figure 4D displays the normalized response in the −20° and 20° channels to both clockwise or counter-c lockwise targets. The

divergence in responses occurs approximately 60 ms before the target onset and extends to 200 ms after the termination of the target. Presumably, the onset of this separation before the onset of the target is related to the 120ms temporal envelope of the wavelet filter that was used to derive the SSVEP response. However, note that the responses are significantly different only 165–255ms after the target onset ($p < .05$), highlighting the high temporal precision of this technique.

Previous electrophysiological studies have examined the time-course of evoked signals when subjects are instructed to attend to specific visual features [e.g, 7, 8, 28–30]. While these studies show that feature-based attention can mediate evoked responses as early as 90ms post-stimulus [8], none of these studies examined how attention shapes feature-selective population response profiles across time. In addition, EEG/MEG activity patterns have been used to infer, or decode, which stimulus feature a subject is viewing [31, 32]. However, they did not examine the influence of cognitive manipulations on the information content of activity patterns, and decoding methods cannot be easily used to infer how the shape of feature-selective response profiles changes with task demands. This is a key advantage of the current approach, as understanding the influence of cognitive demands on information processing in human cortex requires examining *how* the response profile across feature-selective neurons changes over time [33]. In turn, the lack of real-time information about the effects of attention on feature-selective responses in human cortex has contributed to a longstanding debate about the nature of attentional modulation and how it might differ in monkey and man. For instance, previous single-unit recording studies have reported that attention primarily operates via a multiplicative scaling of neural TFs [e.g., 34, 35]. In contrast, fMRI studies have shown that attention primarily induces an additive shift, and that multiplicative gain is relatively weak in comparison [24, 36–38]. The dominance of additive effects in fMRI may reflect the fact that the BOLD response pools responses across a large number of neurons that probably exhibit different degrees of feature-selectivity and attentional modulation. Thus, the aggregate response might look additive as opposed to multiplicative. However, the fact that we see a modulation pattern that more closely resembles the multiplicative scaling observed using single unit recording (Figure 4B), despite the fact that EEG also pools across the responses of large numbers of neurons, suggests instead that BOLD fMRI might be indexing a fundamentally different source of modulation. In addition, the tight correspondence between single-unit recordings and the present DTFs is also encouraging as human subjects can learn complex new experimental paradigms very quickly compared to non-human primates, who often require months of training to successfully perform relatively simple tasks. Thus, the present technique might be used to evaluate information processing in a wide variety of experimental settings, and in a manner that is not influenced by long-term learning effects that might alter the nature of neural activity across the course of months of training.

As EEG has relatively coarse spatial resolution, it is difficult to make a precise statement about the exact cortical area that is driving these feature-selective DTFs (e.g., V1, V2, etc). Our EEG signals reflect synaptic activity synchronized to an external signal (stimulus flicker) but space-averaged on the centimeter scale. In order to focus on early visual areas (rather than parietal or even frontal activity), we specifically entrained EEG signals related to the oriented grating at a high-frequency based on the logic of coupled oscillators [e.g., 39]. This framework asserts that only small local networks can operate at high frequencies whereas larger networks operate at lower frequencies due to transmission delays along axonal fiber systems. Indeed, in another study, the use of lower frequency flicker engages parietal and frontal networks, whose properties are expected to be less closely related to the physical stimulus features, and more closely related to attentional goals [40]. In addition, we observe a tight phase coupling at 42.5Hz across all of the high SNR electrodes, which is consistent with a single cortical source driving the SSVEP response to the flickering grating

(whereas multiple sources should give rise to a phase shift between electrodes, see Supplemental Figure 5). However, even if we are reasonably confident that our SSVEP signals originate from a single source in occipital cortex, the spatial scale of the orientation signals is still not clear. Indeed, the origin of orientation-selective signals measured with other methods such as fMRI is still a matter of active debate. Some researchers propose that orientation-selective response biases are linked to subtle imbalances in the distribution of orientation selective columns within each voxel [1, 41]. In contrast, others have reported a spatial correspondence between large-scale orientation maps and polar angle maps that were identified using standard retinotopic mapping methods [17]. While it is likely that both sources of information contribute to orientation-selective fMRI responses, the existence of large-scale orientation information that spans primary visual cortex should give rise to signals that are capable of driving robust changes in the spatial distribution of SSVEPs. However, this conclusion should be qualified because we cannot rule out contributions from other sources given the limited spatial resolution of the present method. In either case, the present experiment establishes that orientation-selective responses detected with SSVEP provide a useful index to link neural and cognitive levels of information processing.

In sum, the temporal resolution provided by SSVEPs provides a unique method for measuring brain function, and has been previously used to study several distinct cognitive phenomena [9, 42, 43]. Here we exploit the continuous nature of the oscillatory activity elicited by a flickering stimulus and demonstrate that relatively simple models can be used to reconstruct temporally precise orientation-selective response profiles from the distributed pattern of the power and phase of evoked electrical activity across the scalp. This ability is primarily supported by small orientation-selective changes in power across a relatively focal set of occipital-parietal electrodes, with a smaller additional contribution from the phase angle across electrodes in frontal cortex. Importantly, these feature selective response profiles provide high-temporal and high-featural resolution, and are modulated by both task demands (attention) and behavioral performance. These latter demonstrations establish that the tuning functions reflect active cognitive processing and also extend previous single-unit physiology work by linking feature-based attentional modulations with behavior. Compared to fMRI, the spatial resolution of EEG is quite coarse; however, the high temporal resolution and the feature selectivity that we report here represents a significant advance over previous applications of EEG, and provides a near real-time index of neural information processing from human cortex.

EXPERIMENTAL PROCEDURES

Sixteen individuals (8 female) participated in the experiment, and all data was collected at the Perception and Cognition Lab at the University of California, San Diego. All participants provided written informed consent in accordance with the human subjects Institutional Review Board at UCSD. EEG measurements were collected with a dense array NetAmps 300 system made by EGI (Electrical Geodesics, Inc., Eugene, OR) equipped with a 128 channel Hydrocel Geodesic Sensor Net and a photocell system to give accurate and fast sampling of each cycle of the stimulus. The EEG was recorded with a 1000 Hz sampling rate. Stimuli consisted of a square-wave grating that was rendered in a circular annulus (37° diameter vi sual angle) with a central fixation dot (0.4° visual angle) on which subjects were required to maintain gaze (Figure 1). A rapid serial visual presentation (RSVP) stream of letters (8° visual angle) was simultaneously presented at the center of the screen. To delineate neural responses separately for each stimulus (grating versus RSVP stream), stimuli were *tagged* with different flicker frequencies: the annulus was contrast reversed at 21.25 Hz, and the RSVP stream of letters was updated at rate of 12.1 Hz (50% duty cycle). Stimuli were presented on a uniform gray background (43.2 cd/m^2) with a monitor refresh rate of 85 Hz. For 'attend grating' blocks of trials, subjects maintained fixation and attended

to the oriented grating (grating rendered in 1 of 9 possible orientations across trials, 0°–160° in steps of 20°). At some point during each 3000 ms trial, the orientation of the grating would rotate either clockwise or counterclockwise for 235 ms (20 frames), and subjects would report the direction of angular shift with a button press after the end of each trial. Using the method of constant stimuli, performance at 6 orientation deviations was obtained. For the 'attend RSVP' blocks of trials, subjects maintained fixation while attending to the central letter stream. Subjects were instructed to respond to a target letter (X or Y) with a button press after the end of each trial. We adjusted the angular offset of the grating target and the contrast of the letters in a pre-experiment training session to ensure that accuracy on both tasks was ~80% (see Supplemental Methods). To maximize stimulus related activity in the EEG and to ensure that the subjects attended the stimulus for an extended period of time, 80% of the targets were presented 2000 ms or more after the onset of the stimulus.

Each block lasted for approximately 7 minutes and contained 90 trials (10 trials for each of the 9 orientations). Four blocks were run for each of the attention conditions, which took about one hour and yielded 360 trials for each condition (720 total). After standard artifact editing procedures (eye-blink correction, trial rejection, etc., see Supplemental Experimental Procedures) each individual trial was cropped to an integer number of cycles to maximize a narrow band stimulus response. Trials were then Fourier transformed using conventional FFT methods via Matlab and normalized based on a pre-stimulus period of 100 ms.

Decoding analyses were conducted via a linear discriminant analysis to determine whether the orientation of the stimulus could be predicted from the SSVEP response. The number of electrodes included in the classification procedure varied across subjects (see Supplemental Experimental Procedures section entitled *Classification Analysis* and Supplemental Figure 4). The forward encoding model used to generate orientation tuning functions used a method that was similar to previous fMRI studies developed by Brouwer and Heeger [2, 22, 24, 26]. Briefly, let m be the number of EEG elements for an individual subject's dataset and n_1 be the number of trials in the training set (719 trials) and n_2 be the number of observations in the testing set (1 trial). Finally, let k be the number of hypothetical orientation channels (C_1, $k \times n_1$), composed of half-sinusoidal functions raised to the sixth power as the basis set. Let B_1 ($k \times n_1$) be the training set and B_2 ($k \times n_2$) be the test set. The training data in B1 were then mapped onto the matrix of channel outputs (C1) by the weight matrix (W, $m \times k$) that was estimated using a GLM of the form:

$$B_1 = WC_1 \quad (1)$$

where the ordinary least-squares estimate of W is computed as:

$$\widehat{W} = B_1 C_1{}^T (C_1 C_1{}^T)^{-1} \quad (2)$$

The channel responses C_2 ($k \times n_2$) were then estimated based on the test data (B_2) using the weights estimated in (2):

$$\widehat{C_2} = (\widehat{W}^T \widehat{W})^{-1} \widehat{W}^T B_2 \quad (3)$$

This process was then repeated by holding each trial out in turn until all trials had served as a test set. Then, the channel response function on each trial was circularly shifted to a common stimulus-centered reference frame, and these re-centered response functions were averaged across conditions of interest (e.g., attend grating, attend RSVP stream). Thus, by convention the 0° point along the x-axis i n all plots refers to the orientation of the stimulus

that evoked the response profile. The number of EEG elements used for each subject varied slightly across subjects depending just on the number of artifact-free channels (average of 238 elements, 119 SNR and 119 phase angle estimates).

For the creation of DTFs, a separate training/test procedure was run on the power and phase of the SSVEP response at each time point as estimated using a continuous wavelet transform. After this procedure, the channel responses were locked to the target onset (Figures 3, 4). The significance of all of the effects was assessed using a bootstrap procedure and an alpha level of 0.05. Methods are described in more detail in Supplemental Experimental Procedures.

Supplementary Material

Refer to Web version on PubMed Central for supplementary material.

Acknowledgments

References

1. Kamitani Y, Tong F. Decoding the visual and subjective contents of the human brain. Nat Neurosci. 2005; 8:679–685. [PubMed: 15852014]

2. Brouwer GJ, Heeger DJ. Cross-orientation suppression in human visual cortex. J Neurophysiol. 2011; 106:2108–2119. [PubMed: 21775720]

3. Riesenhuber M, Poggio T. Hierarchical models of object recognition in cortex. Nat Neurosci. 1999; 2:1019–1025. [PubMed: 10526343]

4. Kobatake E, Tanaka K. Neuronal selectivities to complex object features in the ventral visual pathway of the macaque cerebral cortex. J Neurophysiol. 1994; 71:856–867. [PubMed: 8201425]

5. Grill-Spector K, Malach R. The human visual cortex. Annu Rev Neurosci. 2004; 27:649–677. [PubMed: 15217346]

6. DiCarlo JJ, Zoccolan D, Rust NC. How does the brain solve visual object recognition? Neuron. 2012; 73:415–434. [PubMed: 22325196]

7. Zhang W, Luck SJ. Feature-based attention modulates feedforward visual processing. Nat Neurosci. 2009; 12:24–25. [PubMed: 19029890]

8. Schoenfeld MA, Hopf JM, Martinez A, Mai HM, Sattler C, Gasde A, Heinze HJ, Hillyard SA. Spatio-temporal analysis of feature-based attention. Cereb Cortex. 2007; 17:2468–2477. [PubMed: 17204821]

9. Andersen SK, Muller MM. Behavioral performance follows the time course of neural facilitation and suppression during cued shifts of feature-selective attention. Proc Natl Acad Sci U S A. 2010; 107:13878–13882. [PubMed: 20643918]

10. Naselaris T, Kay KN, Nishimoto S, Gallant JL. Encoding and decoding in fMRI. NeuroImage. 2010; 56:400–410. [PubMed: 20691790]

11. Tong F, Pratte MS. Decoding patterns of human brain activity. Annu Rev Psychol. 2012; 63:483–509. [PubMed: 21943172]

12. Serences JT, Saproo S. Computational advances towards linking BOLD and behavior. Neuropsychologia. 2012; 50:435–446. [PubMed: 21840553]

13. Haynes JD, Rees G. Decoding mental states from brain activity in humans. Nat Rev Neurosci. 2006; 7:523–534. [PubMed: 16791142]

14. Kamitani Y, Tong F. Decoding seen and attended motion directions from activity in the human visual cortex. Curr Biol. 2006; 16:1096–1102. [PubMed: 16753563]

15. Haynes JD, Rees G. Predicting the orientation of invisible stimuli from activity in human primary visual cortex. Nat Neurosci. 2005; 8:686–691. [PubMed: 15852013]

16. Vanduffel W, Tootell RB, Schoups AA, Orban GA. The organization of orientation selectivity throughout macaque visual cortex. Cereb Cortex. 2002; 12:647–662. [PubMed: 12003864]

17. Freeman J, Brouwer GJ, Heeger DJ, Merriam EP. Orientation decoding depends on maps, not columns. J Neurosci. 2011; 31:4792–4804. [PubMed: 21451017]

18. Norman KA, Polyn SM, Detre GJ, Haxby JV. Beyond mind-reading: multi-voxel pattern analysis of fMRI data. Trends Cogn Sci. 2006; 10:424–430. [PubMed: 16899397]

19. Hubel DH, Wiesel TN. Shape and arrangement of columns in cat's striate cortex. J Physiol. 1963; 165:559–568. [PubMed: 13955384]

20. Blasdel GG, Salama G. Voltage-sensitive dyes reveal a modular organization in monkey striate cortex. Nature. 1986; 321:579–585. [PubMed: 3713842]

21. Miyawaki Y, Uchida H, Yamashita O, Sato MA, Morito Y, Tanabe HC, Sadato N, Kamitani Y. Visual image reconstruction from human brain activity using a combination of multiscale local image decoders. Neuron. 2008; 60:915–929. [PubMed: 19081384]

22. Brouwer GJ, Heeger DJ. Decoding and reconstructing color from responses in human visual cortex. J Neurosci. 2009; 29:13992–14003. [PubMed: 19890009]

23. Kay KN, Naselaris T, Prenger RJ, Gallant JL. Identifying natural images from human brain activity. Nature. 2008; 452:352–355. [PubMed: 18322462]

24. Scolari M, Byers A, Serences JT. Optimal deployment of attentional gain during fine discriminations. J Neurosci. 2012; 32:7723–7733. [PubMed: 22649250]

25. Regan, D. Human brain electrophysiology: evoked potentials and evoked magnetic fields in science and medicine. New York: Elsevier; 1989.

26. Ho T, Brown S, van Maanen L, Forstmann BU, Wagenmakers EJ, Serences JT. The optimality of sensory processing during the speed-accuracy tradeoff. J Neurosci. 2012; 32:7992–8003. [PubMed: 22674274]

27. Scolari M, Serences JT. Adaptive allocation of attentional gain. J Neurosci. 2009; 29:11933–11942. [PubMed: 19776279]

28. Busse L, Katzner S, Treue S. Temporal dynamics of neuronal modulation during exogenous and endogenous shifts of visual attention in macaque area MT. Proc Natl Acad Sci U S A. 2008; 105:16380–16385. [PubMed: 18922778]

29. Mirabella G, Bertini G, Samengo I, Kilavik BE, Frilli D, Della Libera C, Chelazzi L. Neurons in area V4 of the macaque translate attended visual features into behaviorally relevant categories. Neuron. 2007; 54:303–318. [PubMed: 17442250]

30. Chen X, Hoffmann KP, Albright TD, Thiele A. Effect of feature-selective attention on neuronal responses in macaque area MT. J Neurophysiol. 2012; 107:1530–1543. [PubMed: 22170961]

31. Kaneoke Y, Urakawa T, Kakigi R. Visual motion direction is represented in population-level neural response as measured by magnetoencephalography. Neuroscience. 2009; 160:676–687. [PubMed: 19285543]

32. Regan D, Regan MP. Nonlinearity in human visual responses to two-dimensional patterns, and a limitation of Fourier methods. Vision Res. 1987; 27:2181–2183. [PubMed: 3447366]

33. Pouget A, Dayan P, Zemel RS. Inference and computation with population codes. Annu Rev Neurosci. 2003; 26:381–410. [PubMed: 12704222]

34. McAdams CJ, Maunsell JH. Effects of attention on orientation-tuning functions of single neurons in macaque cortical area V4. J Neurosci. 1999; 19:431–441. [PubMed: 9870971]

35. Treue S, Martinez Trujillo JC. Feature-based attention influences motion processing gain in macaque visual cortex. Nature. 1999; 399:575–579. [PubMed: 10376597]

36. Saproo S, Serences JT. Spatial attention improves the quality of population codes in human visual cortex. J Neurophysiol. 2010; 104:885–895. [PubMed: 20484525]

37. Buracas GT, Boynton GM. The effect of spatial attention on contrast response functions in human visual cortex. J Neurosci. 2007; 27:93–97. [PubMed: 17202476]

38. Pestilli F, Carrasco M, Heeger DJ, Gardner JL. Attentional enhancement via selection and pooling of early sensory responses in human visual cortex. Neuron. 2011; 72:832–846. [PubMed: 22153378]

39. Breakspear M, Heitmann S, Daffertshofer A. Generative models of cortical oscillations: neurobiological implications of the kuramoto model. Front Hum Neurosci. 2010; 4:190. [PubMed: 21151358]

40. Bridwell DA, Srinivasan R. Distinct attention networks for feature enhancement and suppression in vision. Psychol Sci. 2012; 23:1151–1158. [PubMed: 22923337]

41. Swisher JD, Gatenby JC, Gore JC, Wolfe BA, Moon CH, Kim SG, Tong F. Multiscale pattern analysis of orientation-selective activity in the primary visual cortex. J Neurosci. 2010; 30:325–330. [PubMed: 20053913]

42. Vialatte FB, Maurice M, Dauwels J, Cichocki A. Steady-state visually evoked potentials: focus on essential paradigms and future perspectives. Prog Neurobiol. 2009; 90:418–438. [PubMed: 19963032]

43. Nunez, PL.; Cutillo, BA. Neocortical dynamics and human EEG rhythms. New York: Oxford University Press; 1995.

HIGHLIGHTS

- Evaluating the temporal dynamics of neural processing is crucial for understanding cognitive processes.

- SSVEP measurements may be used to reconstruct orientation selective response profiles at a sub-second scale.

- This approach provides a metric that can rapidly track information processing in human cortex.
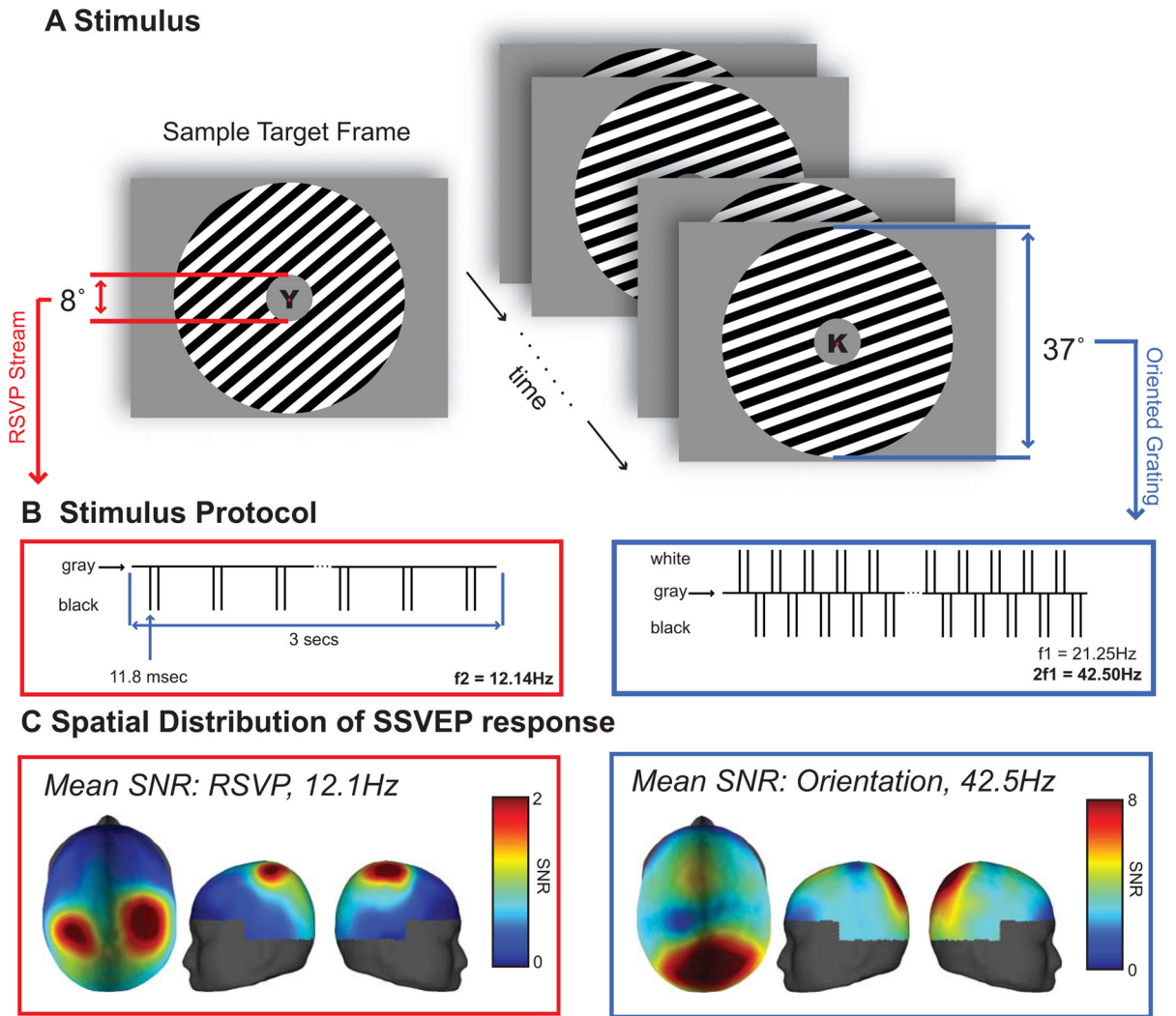
A Stimulus

B Stimulus Protocol

C Spatial Distribution of SSVEP response

Figure 1.
(A) Stimulus display: In the central location, a stream of letters was simultaneously presented with an oriented peripheral annulus on a uniform gray background. During the 3000 ms trial, a target would appear as a shift in the orientation of the grating or an X,Y in the RSVP stream of letters. Subjects responded with a button press to the direction of the shift (clockwise/counter-clockwise) or to the target letter (X,Y). (B) Stimulus protocol: stimuli were tagged with different flicker frequencies. The annulus was contrast reversed at 21.25 Hz, and the RSVP stream of letters was updated at rate of 12.1 Hz (50% duty cycle). (C) Mean of the SNR across subjects of the SSVEP responses to the flickering stimuli, calculated by dividing the power at the stimulus frequency (or the second harmonic of the stimulus frequency for the peripheral grating, see Experimental Methods) by the standard deviation of the surrounding frequencies, 6.7 Hz on each side of the stimulus frequency). Spatial distributions reflect a parietal-occipital response for the grating stimulus and a bilateral parietal response for the RSVP stimulus.
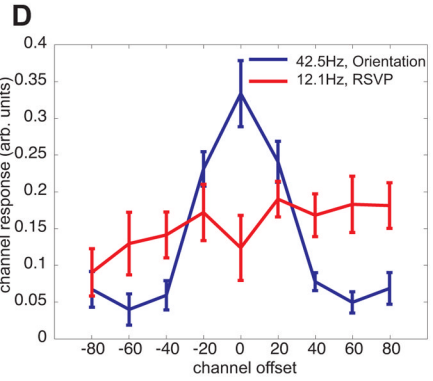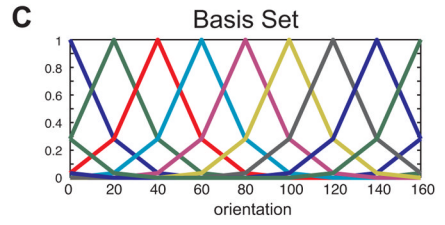
Classification Results

A Classification Performance

Forward Encoding Model Results

C Basis Set

B Diagnostic Electrodes

D
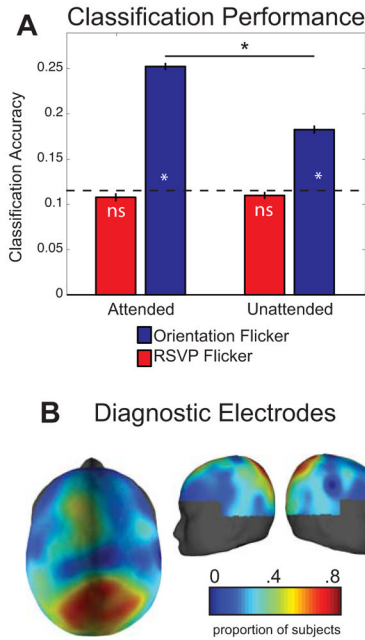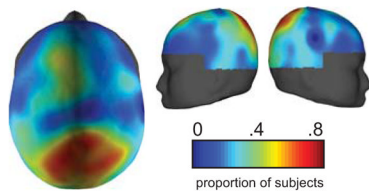
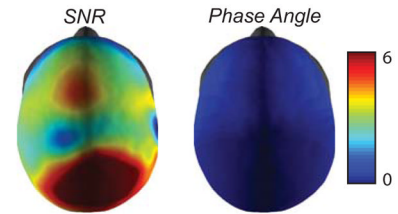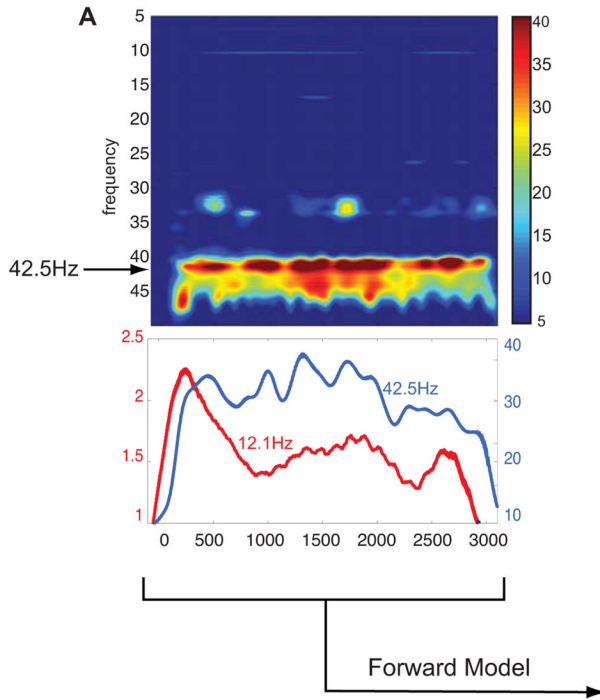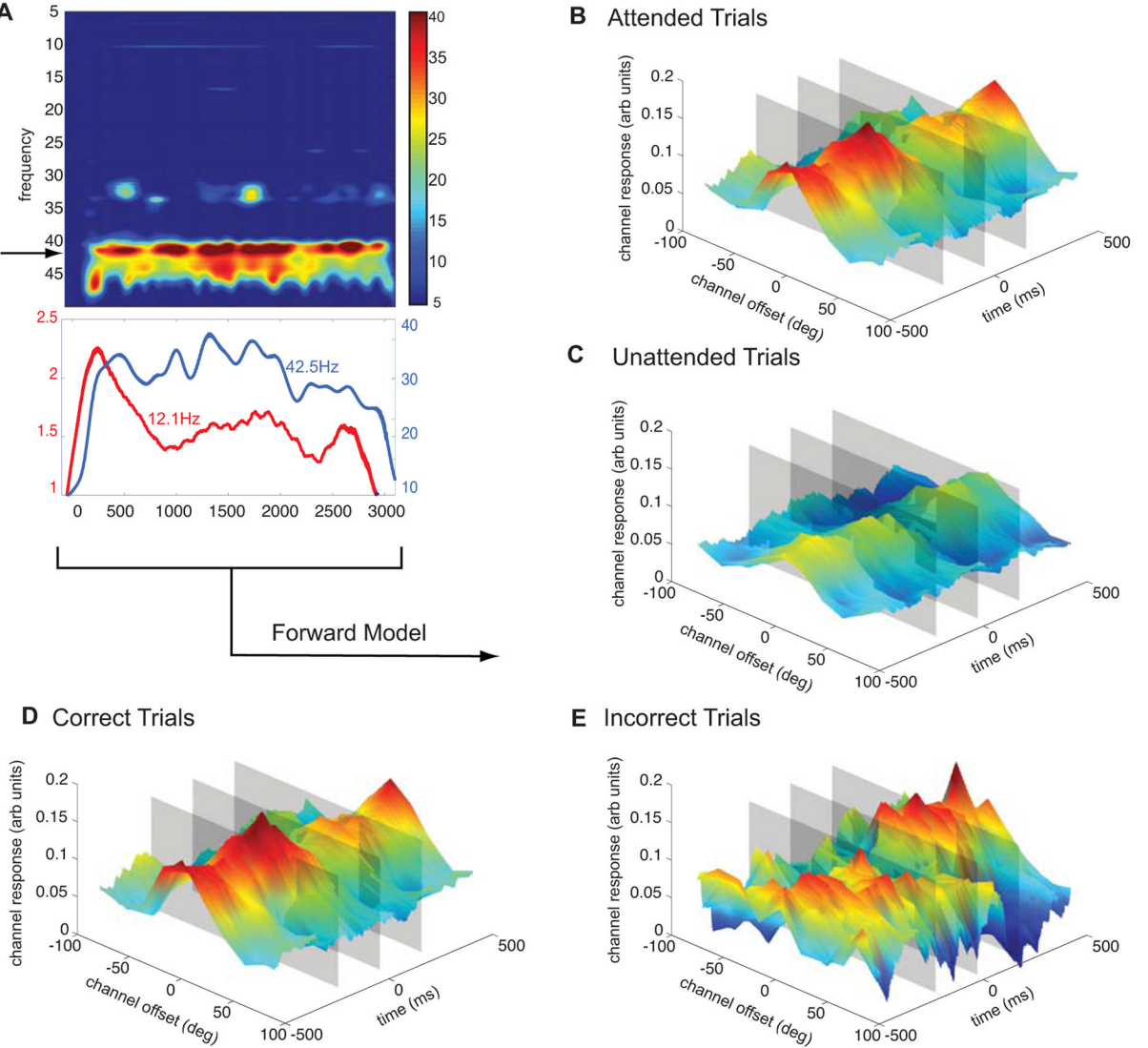**E** Weight Matrices of EEG Features

Figure 2.
(A) Linear discriminant classification results. For each subject, the SNR and phase of a subset of electrodes elements was used for the classification procedure, and the peak of the classification function was used as that subject's classification performance (see Supplemental Figure 4 and Supplemental Methods). The orientation of the grating could be decoded above chance ($p<0.05$) based on the SSVEP response at 42.5Hz (Figure 2A, blue bars), and decoding accuracy was higher when the grating was attended compared to when it was not attended. In contrast, the orientation of the peripheral grating could not be decoded based on the SSVEP response at 12.1Hz (red bars). The dotted line represents chance performance in this 9-way classification, and error bars represent standard error of the mean across subjects. Asterisks indicate significant differences via a bootstrap procedure (see Supplemental Experimental Procedures). (B) Diagnostic electrodes in the linear discriminant analysis across subjects: the colormap of the topographic plot shows the probability that an electrode was used in the decoding analysis. The electrodes that contained the highest SNR (Figure 1C) were also the most diagnostic. (C) Basis set used in the forward encoding model, derived from half-sinusoidal functions raised to the sixth power (9 basis functions spanning 0°–160° in 20° steps). (D) Dynamic tuning functions derived using the forward encoding model based on SNR and phase angle of the SSVEP response before the target onset. The 12.1 Hz SSVEP response to the RSVP flicker does not produce tuned responses whereas the 42.5Hz SSVEP response produces a tuned response that peaks at the angle of stimulus being viewed (which is 0° in this plot by convention). Error bars represent standard error of the mean across subjects. (E) Average weight of the maximum channel response

showing that the SNR of the parietal-occipital electrodes and, to a lesser extent the phase angle of the frontal electrodes, carries most of the orientation-selective information.

Wavelet Decomposition

A

DTFs Across Time

B Attended Trials

C Unattended Trials

Forward Model

D Correct Trials

E Incorrect Trials

Figure 3.
Dynamic Tuning Functions. (A) A wavelet decomposition of frequencies 5–50Hz averaged across subjects and conditions. Lower plot shows a line plot of stimulus related responses (RSVP stream: 12.1Hz, Oriented Grating: 42.5Hz). (B–E) Forward encoding model results derived from a wavelet decomposition of the SSVEP response. Using SNR and phase angle of the SSVEP response, locked to the target onset (500ms before to 500ms after), orientation response profiles were reconstructed as a function of time. Segregating trial types reveals differences between responses to attended stimuli (B) and unattended stimuli (C) as well as between correct trials (D) and incorrect trials (E). Gray planes mark time points of interest (200ms before target onset, target onset, and target termination, see Figure 4).
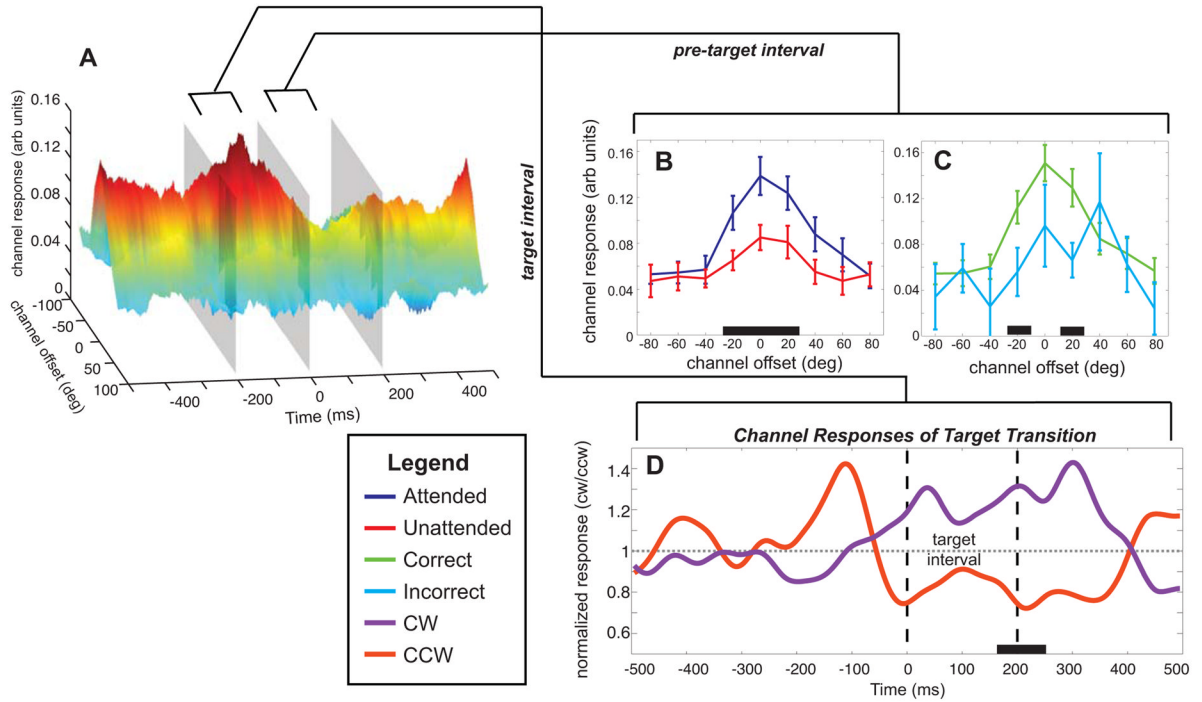
Figure 4.
(A) Rotated view of Figure 3D (correct attended trials). Each inset line plot shows the tuning functions derived from the time window 200ms before target onset (B, C). These line plots display the effect of attention (B) and the effect of accuracy (C). Significant differences between channel responses indicated by black bars on the x-axis. (D) Normalized response in channels tuned 20° and −20°) separated by clockwise or counterclockwise target shifts. These responses show a shift in the response beginning 60ms before target onset extending 400 ms after target onset. Significant divergence occurs between 165 and 255 ms after target onset (black bar on x-axis).